

Multibody Analysis and Control of a Full-Wrist Exoskeleton for Tremor Alleviation

Jiamin Wang

Department of Mechanical Engineering,
Virginia Tech Blacksburg,
Blacksburg, VA 24061

Oumar R. Barry¹

Department of Mechanical Engineering,
Virginia Tech Blacksburg,
Blacksburg, VA 24061
e-mail: obarry@vt.edu

Uncontrollable shaking in the human wrist, caused by pathological tremor, can significantly undermine the power and accuracy in object manipulation. In this paper, the design of a tremor alleviating wrist exoskeleton (TAWE) is introduced. Unlike the works in the literature that only consider the flexion/extension (FE) motion, in this paper, we model the wrist joint as a constrained three-dimensional (3D) rotational joint accounting for the coupled FE and radial/ulnar deviation (RUD) motions. Hence TAWE, which features a six degrees-of-freedom (DOF) rigid linkage structure, aims to accurately monitor, suppress tremors, and provide light-power augmentation in both FE and RUD wrist motions. The presented study focuses on providing a fundamental understanding of the feasibility of TAWE through theoretical analyses. The analytical multibody modeling of the forearm-TAWE assembly provides insight into the necessary conditions for control, which indicates that reliable control conditions in the desired workspace can be acquired by tuning the design parameters. Nonlinear regressions are then implemented to identify the information that is crucial to the controller design from the unknown wrist kinematics. The proposed analytical model is validated numerically with V-REP and the result shows good agreement. Simulations also demonstrate the reliable performance of TAWE under controllers designed for tremor suppression and movement assistance.

[DOI: 10.1115/1.4047424]

1 Introduction

In the past several decades, the scientific community has paid considerable attention to the alleviation of pathological tremors (e.g., essential tremor [1,2] and Parkinson's disease [3,4]) caused by neurological disorders. These tremors manifest as an uncontrollable shaking of the limbs, which greatly reduces the quality of life for millions of people worldwide. Specifically, reduced stability and accuracy of human motion due to tremors will cause difficulties in leg locomotion, body support, and object manipulation. Since a large population of patients suffering from these diseases (especially Parkinson's disease) are of middle and older age, the consequences of tremors have life-threatening ramifications such as falling and slipping [5]. Researchers from various fields have been exploring solutions to these illnesses. In addition to pharmacological and surgical intervention, rehabilitation devices [6,7] have been developed to externally alleviate tremors. Recent breakthroughs in mechatronics and robotic technology have made the development of smart, versatile, and adaptive devices possible, which include robotic orthoses and exoskeletons. For the upper limb (elbow, forearm, wrist, etc.), a number of devices including DRIFTS [8], WOTAS [9], the work by Taheri [10], and the work by Huen et al. [11] have successfully reduced tremors by actively applying control forces/torques on human joints. To realize this, the assessment of tremor information is necessary. As tremors are generally considered roughly rhythmic and oscillatory [12], the commonly adopted tremor modeling and control frameworks implement motion filters (e.g., weighted-frequency Fourier linear combiner (WFLC) [13], band-limited multi-Fourier linear combiner (BMFLC) [14], autoregression [15,16], and their combinations) that are capable of separately extracting voluntary and tremorous motions from human movement signals. Various tremor attenuating controllers (passive impedance control, active

vibration canceling [9,10,13], etc.) are then implemented based on the filtered tremor data.

The ability to precisely control the human wrist is crucial to object manipulation in daily life. The wrist joint is categorized as an ellipsoidal/condyloid joint—a constrained three-dimensional (3D) rotational joints with two main degrees-of-freedom (DOF) [17]: flexion/extension (FE) and radial/ulnar deviation (RUD). Both FE and RUD are essential DOFs that can be affected by tremors. While the wrist tremor can be better studied and suppressed in terms of both FE and RUD, the kinematics of the two wrist DOFs are complicated. Unlike artificial mechanical joints (universal joint, ball joint, etc.), the wrist joint is realized with a complicated bone structure [18], which does not indicate the exact positions of the rotation axes. According to the studies, the axes locations are approximately demonstrated in Fig. 1. In addition to the offset, the FE and RUD motions may also couple with translational displacements. Finally, the wrist kinematic profile varies among individuals. For some Parkinson's disease patients who suffer muscle deformations [19], the rehabilitation device designed based on a standard fix profile may have limited functionalities. The aforementioned tremor suppression orthoses and

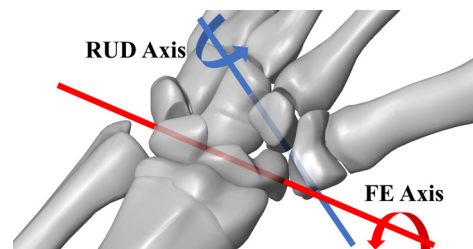


Fig. 1 Approximate locations of FE and RUD rotation axes [18] on the wrist of a left forearm

¹Corresponding author.

Manuscript received December 24, 2019; final manuscript received May 25, 2020; published online September 8, 2020. Assoc. Editor: Tamara Reid Bush.

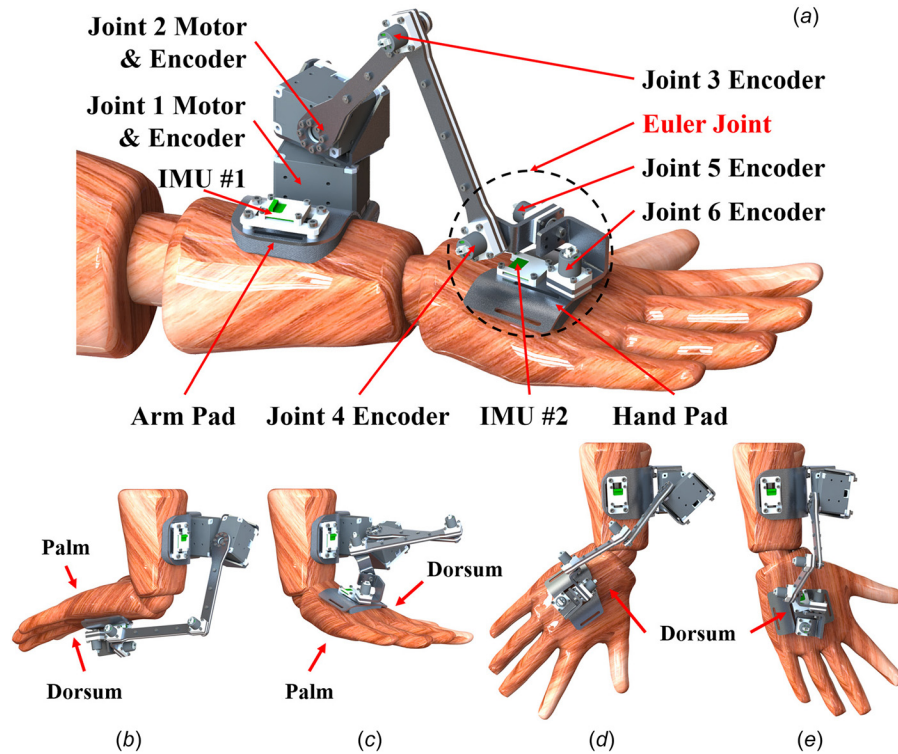


Fig. 2 The overview of TAWE installed on a right forearm mannequin, where (a) shows the mechanism design with all the major components labeled. The standard poses of TAWE at different wrist position is shown in: (b) -75 deg in FE (flexion); (c) 75 deg in FE (extension); (d) -45 deg in RUD (ulnar deviation); and (e) 25 deg in RUD (radial deviation). In (b)–(e), the palm and dorsum of the right hand are pointed out.

exoskeletons either do not interface with or provide full actuations to all of the wrist DOFs, or they may restrict natural wrist motions due to the constraints from artificial mechanical joints. Other rehabilitation devices (e.g., RiceWrist [20], OpenWrist [21], and (CADEN)-7 [22]) that can provide actuation to both FE and RUD motions, but very few of them are designed for tremor assessment and alleviation during object manipulation.

The novelty of this paper is taking into consideration the coupled wrist FE and RUD motions in the design of a wearable full-wrist robotic device for tremor control. Unlike the aforementioned forearm devices that mainly focus on the tremor suppression in the FE motion, the tremor alleviating wrist exoskeleton (TAWE), which is first introduced in our conference paper [23], aims to provide tremor alleviation solutions to both FE and RUD without constraining the natural wrist motion. The presented study focuses on providing a fundamental understanding of the feasibility of TAWE through theoretical analyses. As a self-contained extension of our conference paper, this paper proposes an updated design of TAWE with a better customizable mechanism. Also, the current paper presents an extensive investigation in the dynamics, kinematic identification, and control of the forearm–TAWE assembly. The multibody methods used in this paper are applicable not only in the modeling and analysis of the proposed design, but also in the development of similar wearable rehabilitation devices. The design features and mechatronic system setup of TAWE are briefly introduced in Sec. 2. Based on a few reasonable assumptions, the theoretical analysis aims to achieve the following objectives:

- (1) Obtaining a fundamental understanding of the dynamics and necessary control conditions through the modeling of the forearm–exoskeleton system, which is elaborated in Sec. 3.
- (2) Based on the kinematic model, studying possible design parameters that improve control conditions, and exploring

a regression model for wrist kinematics identification, which are discussed in Sec. 4.

- (3) Developing controllers for tremor suppression and light-power motion augmentation, which is explained in Sec. 5.

Simulations are carried out in Sec. 6 to validate the theoretical results, and demonstrate the performance of kinematic regression and control. Finally, Sec. 7 concludes the findings of the paper and discussed future study directions.

2 The Design of Tremor Alleviating Wrist Exoskeleton

The TAWE is a wearable robotic rehabilitation device designed to provide full-wrist motion measurement, tremor suppression, and light-power movement assistance. An essential requirement of TAWE is to allow the exoskeleton to follow the motion of the user. As the exact 3D kinematics of the wrist of the user is initially assumed to be unknown, the hand and the forearm are treated as two individual bodies in 3D space. This indicates that an exoskeleton that links the two bodies requires at least 6DOFs to ensure completely unconstrained wrist motion.

To this end, TAWE shown in Fig. 2(a) has adopted a 6DOF rigid linkage mechanism with two of the DOFs actuated. Similar mechanisms [24,25] were adopted in the measuring tool designs for the kinematic identification of the wrist joint, which however did not provide any actuation. A rigid mechanism is efficient in force/torque transmission, and it can also be reliably modeled, measured, and controlled. A 6DOF mechanism is also highly tolerant toward slight relative motions between the user and the equipped device. Compared to the previous version of TAWE [23], the design in Fig. 2(a) is updated to allow more customization in the linkage dimensions. By adopting off-the-shelf and standard mechanical components, the design weighs 350 grams excluding the power supply and electronic control system, which

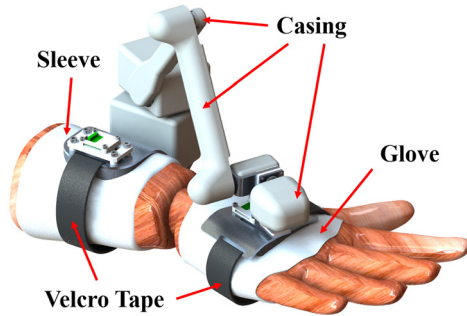


Fig. 3 The attachment of TAWE to a right forearm mannequin model via sleeve, glove, and Velcro tapes. The mechanisms and sensor are covered by safe casings.

can be further lowered by design specialization and optimization. A combination of aluminum alloy and plastic is adopted to ensure structural strength while providing lightness. The standard poses of the exoskeleton are shown in Figs. 2(b)–2(e). By assuming the current mannequin wrist as a common ball-socket joint, the exoskeleton can reach -75deg to 75deg in FE and -45deg to 25deg in RUD without geometric collision between parts.

The forearm and hand attachment pads are, respectively, located at the base and the end of TAWE. The forearm pad is attached to the end of the forearm, and the hand pad is attached to the hand dorsum. As demonstrated in Fig. 3, sleeves, gloves, and Velcro tapes can be installed with the attachment pads for the user to convenient equip the device without extreme tight-fitting or precise positioning. These setups allow the users to freely use their fingers and palms, and perform some tasks in daily life. The designs of the attachment pads and the dimensions of all mechanism linkages can be customized to better fit with the user profile (size, range of motion, etc.). The design of TAWE can also be improved using safe casings with smooth and soft surfaces to cover the mechanism, sensors, and electrical wiring.

The positional sensors used in the exoskeleton are absolute rotary encoders (US Digital MAE3) installed at the revolute joints, and the two inertial measurement units (IMU) (MPU 9250) fixed on the forearm and hand pads. All of these sensors can reach a measurement resolution higher than 0.1 deg , which is sufficient for wrist motion measurement in tremor control. This setup provides two different measurements of the orientation difference between the hand and the forearm. As the base of the exoskeleton is attached close to the tip of the forearm, the orientation difference of IMUs 1 and 2 are not affected by the supination/pronation in the forearm. The fusion of the two measurements will hence provide accurate assessments of the user motion and tremor dynamics [26]. The maximum torque provided by each servomotor (1.5N·m from Dynamixel XL-430) can be further limited through both hardware and software to avoid excessive load being exerted on the user.

3 Modeling the Forearm–Exoskeleton Dynamics

The feasibility of TAWE cannot be proved only by its design and manufacturability. The control system is the other essential element for the successful implementation of TAWE. The design has been updated by including offsets between the axes of the Euler joints (joints 4, 5, and 6 labeled in Fig. 2(a)), the dynamical model of the linked forearm–exoskeleton system is re-established based on the following model assumptions:

ASSUMPTION 1. The forearm is approximated as a rigid body model. The deformations of the soft body parts are omitted.

ASSUMPTION 2. Muscle actuation forces are generalized into direct forces/torques acting at joints.

ASSUMPTION 3. The supination joint in the forearm is fixed.

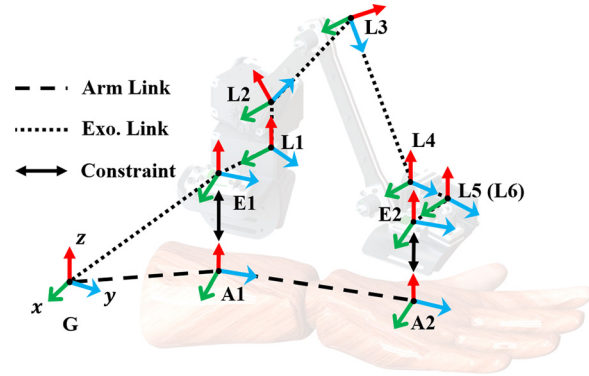


Fig. 4 Overview of the kinematics of the forearm and TAWE, where the coordinate frames are labeled and the link between the frames are marked

3.1 Kinematics of Forearm and Tremor Alleviating Wrist Exoskeleton.

The modeling of the forearm–exoskeleton system begins from the two subsystems—the forearm and the exoskeleton, which are both modeled as floating base systems to allow base actuation and excitation. Figure 4 shows the main coordinate frames declared in the two subsystems and the links between the frames. Here, frames A1 and A2 are defined in the forearm subsystem for IMUs 1 and 2, respectively. Similarly, frames E1 and E2 are the coordinate frames, respectively, for IMUs 1 and 2 in the exoskeleton subsystem. Frames A1 and E1 are also assigned as the floating bases of the two subsystems, whose coordinates δ_a and δ_e are, respectively, defined in the time-derivative form as

$$\dot{\delta}_a = [\dot{\rho}_a^T \ \omega_a^T]^T; \quad \dot{\delta}_e = [\dot{\rho}_e^T \ \omega_e^T]^T \quad (1)$$

where $\rho \in \mathbb{R}^3$ is the translational position defined in the global frame (frame G), and the $\omega \in \mathbb{R}^3$ is the angular velocity defined in the base frame of each subsystem. The orientation of the forearm and TAWE floating bases are, respectively, represented by unit quaternion vectors $\xi_a \in \mathbb{R}^4$ and $\xi_e \in \mathbb{R}^4$. Unlike Euler Angles, the orientation formulation based on quaternion can avoid singularities, thus leading to more stable dynamical modeling [27].

The kinematics of the exoskeleton can be directly acquired from the design, while the transformation between frames A1 and A2 will vary among different users, which is assumed initially unknown. The homogeneous transformations (from frame i to frame j) are represented by the matrices

$$T_{ij} = \begin{bmatrix} R & d \\ 0_{1 \times 3} & 1 \end{bmatrix} = T_{ji}^{-1}; \quad T_{ji} = \begin{bmatrix} R^T & -R^T d \\ 0_{1 \times 3} & 1 \end{bmatrix} \quad (2)$$

where $R \in \mathbb{R}^{3 \times 3}$ and $d \in \mathbb{R}^3$ are the rotation matrix and translational displacement. The transformations between the frames in the exoskeleton kinematic chain are demonstrated in Table 1, where the default parameters of the design are also included. In the table, the terms marked as $d_{k,i}$ and R_k stand for the translation and rotation along the k axis (in transformation i), respectively. The generalized coordinates of the forearm and exoskeleton subsystems are defined as $\theta_a = [\theta_{a,1}, \theta_{a,2}]^T \in \mathbb{R}^2$ and $\theta_e = [\theta_{e,1}, \theta_{e,2}, \theta_{e,3}, \theta_{e,4}, \theta_{e,5}, \theta_{e,6}]^T \in \mathbb{R}^6$ which are the wrist rotation and joint angles, respectively. Any d or R is constant if it is not a function of θ , δ , or ξ .

By employing fixture constraints between frames A1 and E1, and between frames A2 and E2, a closed kinematic chain is formed. IMU 1 provides the measurement of ξ_e and ρ_e , which are now equivalently ξ_a and ρ_a , respectively. The measurement of ξ_e and ρ_e can be obtained by two approaches—the kinematic chain of TAWE and the difference between IMUs 1 and 2 measurements. Therefore, the wrist transformation can be written as

Table 1 Properties of homogeneous transformations between coordinate frames, where the numerical values are the default design parameters of TAWE.

From	To	Translation (d)	Rotation (R)
G	E1	$d_e = \rho_e$	$R_e(\xi_e)$
E1	L1	$d_1 = [-6.8; 1.2; 0]$ cm	$R_1 R_z(\theta_{e,1})$
L1	L2	$d_{z,2} = 2.15$ cm	$R_x(\theta_{e,2})$
L2	L3	$d_{y,3} = 12$ cm	$R_x(\theta_{e,3})$
L3	L4	$d_{y,4} = 12$ cm	$R_x(\theta_{e,4})$
L4	L5	$d_{y,5} = 3$ cm	$R_y(\theta_{e,5})$
L5	L6	$d_{x,6} = 1$ cm	$R_z(\theta_{e,6})$
L6	E2	$d_7 = [0; -3; -0.5]$ cm	R_7
G	A1	$d_a = \rho_a$	$R_a(\xi_a)$
A1	A2	$d_w(\theta_a)$	$R_w(\theta_a)$

$$T_{A1,A2} = \begin{bmatrix} R_w & d_w \\ 0_{1 \times 3} & 1 \end{bmatrix} = \begin{bmatrix} R_a^T R_{A2} & R_a^T(\rho_{A2} - \rho_a) \\ 0_{1 \times 3} & 1 \end{bmatrix} \\ = T_{E1,E2}(\theta_e) = \begin{bmatrix} R_{E1,E2} & d_{E1,E2} \\ 0_{1 \times 3} & 1 \end{bmatrix} \quad (3)$$

where ξ_{A2} and ρ_{A2} are, respectively, the orientation quaternion and translational position of frame A2 measured by IMU 2 with respect to frame G; $R_{E1,E2}(\theta_e)$ and $d_{E1,E2}(\theta_e)$ are functions of θ_e ; and $R_{A2}(\xi_{A2})$ is the rotation matrix converted from ξ_{A2} . As previously mentioned, the above relationship allows the implementation of Kalman filter to obtain a better estimation of R_w and d_w . Furthermore, there also exist an Euler/Cardan angle vector Θ that can represent the rotation R_w , which can be calculated by

$$R_w = R_\Theta(\Theta) = R_a^T R_{A2} \quad (4)$$

Specifically, the elements of Θ are

$$\Theta = [\theta_x \quad \theta_y \quad \theta_z]^T \quad (5)$$

where θ_x , θ_y , and θ_z are the Euler angles rotating around the x , y , and z axes, respectively. An important note is that Θ is dependent on the rotation sequence of the Euler angle. The default Euler angle sequence used in this paper is the intrinsic z - y - x sequence [27].

There exist multiple candidates for θ_a provided that they can characterize the translation d_w and the rotation R_w in the wrist joint. For convenience, $\theta_{a,1}$ and $\theta_{a,2}$ are interpreted by default as values that quantify the RUD and FE motions, respectively. The wrist joint, Θ , and θ_a will be explained with more detail in the wrist kinematic analysis in Sec. 4.

3.2 Subsystem Dynamics and Coupled Model. Based on the kinematic model introduced above, the individual dynamics of the two subsystems can be modeled. The forearm subsystem has three bodies in total—the forearm, wrist, and hand. As the floating base of the forearm subsystem is selected on frame A1, the equations of motion can then be presented in the following nonholonomic equations [28]:

$$q_a = [\theta_a^T \quad \delta_a^T]^T \\ M_a(q_a, \xi_a) \ddot{q}_a = H_a(q_a, \dot{q}_a, \xi_a) + J_{u,a}^T(q_a, \xi_a) u_a \\ + W_a^T(q_a, \xi_a) w_a + J_{\lambda,a}^T \lambda \quad (6a)$$

$$\dot{\xi}_a = \frac{1}{2} \xi_a \times [0 \quad \omega_a^T]^T \quad (6b)$$

where $q_a \in \mathbb{R}^8$ is the generalized coordinates of the forearm subsystem; $u_a \in \mathbb{R}^8$ is the generalize human muscle input exerted at the floating base coordinates and the wrist joint based on Assumption 2; $w_a \in \mathbb{R}^8$ is the disturbance/perturbation; $M_a \in \mathbb{R}^{8 \times 8}$ is the inertia matrix composed from the three bodies in the system; $H_a \in \mathbb{R}^8$ is the internal generalized force that includes Coriolis, centripetal, potential, and damping forces; and $J_{u,a} \in \mathbb{R}^{8 \times 8}$ and $W_a \in \mathbb{R}^{8 \times 8}$ are, respectively, the Jacobian matrices for u_a and w_a .

Similarly, for the exoskeleton subsystem, the floating base is selected on frame E1. The exoskeleton has seven bodies in total—the base and the six structural frames from the rigid-linkage mechanism. The equations of motion of TAWE can be written as

$$q_e = [\theta_e^T \quad \delta_e^T]^T \\ M_e(q_e, \xi_e) \ddot{q}_e = H_e(q_e, \dot{q}_e, \xi_e) + J_{u,e}^T(q_e, \xi_e) u_e + J_{\lambda,e}^T \lambda \quad (7a)$$

$$\dot{\xi}_e = \frac{1}{2} \xi_e \times [0 \quad \omega_e^T]^T \quad (7b)$$

where $q_e \in \mathbb{R}^{12}$ is the generalized coordinates of the TAWE subsystem; and $u_e \in \mathbb{R}^2$ is the exoskeleton actuation inputs. The definition of the rest of the terms are similar to that in Eq. (6), except that no disturbance/perturbation is assumed to exist in the exoskeleton subsystem. Note that from the design of TAWE, $J_{u,e}$ can be obtained as

$$J_{u,e} = [I_e \quad 0_{2 \times 10}] \quad (8)$$

since u_e only applies torque to $\theta_{e,1}$ and $\theta_{e,2}$.

In the two subsystems, the constraint force (Lagrangian Multiplier) $\lambda \in \mathbb{R}^{12}$ fully constrains the exoskeleton on to the forearm. The Jacobian matrices $J_{\lambda,a} \in \mathbb{R}^{12 \times 8}$ and $J_{\lambda,e} \in \mathbb{R}^{12 \times 12}$ are calculated from

$$J_\lambda = [J_{\lambda,a} \quad J_{\lambda,e}]; \quad \dot{r}_\lambda = J_\lambda(q, \xi) \dot{q} \quad (9)$$

where the expression of the constraint vector $r_\lambda \in \mathbb{R}^{12}$ is determined by Eq. (3) as

$$r_\lambda = \begin{bmatrix} r_{\lambda,\rho,1} \\ r_{\lambda,\xi,1} \\ r_{\lambda,\rho,2} \\ r_{\lambda,\xi,2} \end{bmatrix} = \begin{bmatrix} \rho_a - \rho_e \\ [0_{3 \times 1} \quad I_3](\xi_a \times \bar{\xi}_e) \\ d_w - d_{E1,E2} \\ [0_{3 \times 1} \quad I_3](\xi_w \times \bar{\xi}_{E1,E2}) \end{bmatrix} \quad (10)$$

where $\bar{\xi}_w$ and $\bar{\xi}_{E1,E2}$ are, respectively, the unit quaternions converted from R_w and $R_{E1,E2}$. Since frames A1 and E1 are the floating bases, and the constraints between frames A2 and E2 only involve θ_a and θ_e , the Jacobian matrices can be decomposed as

$$J_{\lambda,a} = \begin{bmatrix} 0_{6 \times 2} & J_{\lambda,a,r} \\ J_{\lambda,a,s} & 0_{6 \times 6} \end{bmatrix}; \quad J_{\lambda,e} = \begin{bmatrix} 0_{6 \times 6} & J_{\lambda,e,r} \\ J_{\lambda,e,s} & 0_{6 \times 6} \end{bmatrix} \quad (11)$$

where $J_{\lambda,e,r}$ and $J_{\lambda,e,s}$ are invertible since $J_{\lambda,e}$ has full rank as required by the constraints. This implies that the kinematics of exoskeleton (q_e , \dot{q}_e , and ξ_e) can be fully expressed in terms of q_a , \dot{q}_a , and ξ_a , which leads to

$$\dot{q}_e = -J_{\lambda,e}^{-1} J_{\lambda,a} \dot{q}_a; \quad \dot{\xi}_e = \dot{\xi}_a \quad (12)$$

with $J_{\lambda,e}^{-1} J_{\lambda,a}$ calculated as

$$J_{\lambda,e}^{-1} J_{\lambda,a} = \begin{bmatrix} J_{\lambda,e,s}^{-1} J_{\lambda,a,s} & 0_{6 \times 6} \\ 0_{6 \times 2} & J_{\lambda,e,r}^{-1} J_{\lambda,a,r} \end{bmatrix} \quad (13)$$

Differentiating Eq. (12) with respect to time yields

$$\ddot{q}_e = -J_{\lambda,e}^{-1}(J_{\lambda,a}\ddot{q}_a + \dot{J}_{\lambda,a}\dot{q}_a - \dot{J}_{\lambda,e}J_{\lambda,e}^{-1}J_{\lambda,a}\dot{q}_a) \quad (14)$$

Therefore, the dynamics between the two subsystems can be coupled by preserving the generalized coordinates of the forearm. By calculating the constraint force

$$\lambda = -J_{\lambda,e}^{-T}(M_e J_{\lambda,e}^{-1}(J_{\lambda,a}\ddot{q}_a + \dot{J}_{\lambda,a}\dot{q}_a - \dot{J}_{\lambda,e}J_{\lambda,e}^{-1}J_{\lambda,a}\dot{q}_a) + H_e + J_{u,e}^T u_e) \quad (15)$$

The combined multibody system with the generalized coordinate q_a can be calculated as

$$\begin{aligned} & (M_a + J_{\lambda,a}^T J_{\lambda,e}^{-T} M_e J_{\lambda,e}^{-1} J_{\lambda,a}) \ddot{q}_a \\ & = H_a + J_{u,a}^T u_a + W_a^T w_a - J_{\lambda,a}^T J_{\lambda,e}^{-T} H_e - J_{\lambda,a}^T J_{\lambda,e}^{-T} J_{u,e}^T u_e \\ & \quad - J_{\lambda,a}^T J_{\lambda,e}^{-T} M_e J_{\lambda,e}^{-1} (J_{\lambda,a}\dot{q}_a - \dot{J}_{\lambda,e}J_{\lambda,e}^{-1}J_{\lambda,a}\dot{q}_a) \end{aligned} \quad (16a)$$

$$\dot{\xi}_a = J_{\xi_a}(q_a, \xi_a)\dot{q}_a \quad (16b)$$

Since M_a and M_e are positive definite as defined by the multibody model, this results in a new inertia matrix $M = M_a + J_{\lambda,a}^T J_{\lambda,e}^{-T} M_e J_{\lambda,e}^{-1} J_{\lambda,a}$ that is also positive definite.

3.3 Human Motion, Stiffness, and Tremor Dynamics.

Equation (16) follows the general formulation process and only contains basic system characteristics. Since the exoskeleton is designed to follow human motions, we assume that the muscle input u_a is generated by a model-based controller consisted of nonlinear feedforward and feedback control terms, which can also adapt to changes in system inertia and the internal forces, which includes the exoskeleton and external loads.

The 8DOF system in Eq. (16) can be fully actuated by the muscle control input u_a . It is possible to define the output $y_a \in \mathbb{R}^8$ of the muscle control system in the nonholonomic form as

$$\dot{y}_a = J_{h,a}(q_a, \xi_a)\dot{q}_a; \quad \dot{y}_a = J_{h,a}\dot{q}_a + \dot{J}_{h,a}\dot{q}_a \quad (17)$$

with

$$J_{h,a} = \begin{bmatrix} I_5 & 0_{5 \times 3} \\ 0_{3 \times 5} & J_{h,a,\xi}(q_a, \xi_a) \end{bmatrix} \quad (18)$$

where $J_{h,a,\xi} \in \mathbb{R}^{3 \times 3}$ is the Jacobian matrix calculated from the quaternion controller output

$$y_{a,\xi} = [0_{3 \times 1} \quad I_3](\xi_a \otimes \bar{\xi}_{r,a}(t)); \quad J_{h,a,\xi} = \partial \dot{y}_{a,\xi} / \partial \omega_a \quad (19)$$

with $\xi_{r,a} \in \mathbb{R}^4$ as the quaternion reference as a function of time t . Furthermore, the output reference $r_{h,a} \in \mathbb{R}^8$ as a function of time is defined as

$$r_{h,a}(t) = [\theta_{r,a}^T(t) \quad \rho_{r,a}^T(t) \quad 0_{1 \times 3}]^T \quad (20)$$

where $\theta_{r,a} \in \mathbb{R}^2$ is the wrist joint tracking reference; and $\rho_{r,a} \in \mathbb{R}^3$ is the forearm translational position tracking reference. The above setups lead to the muscle control input calculated as

$$\begin{aligned} u_a & = J_{u,a}^{-T}(M J_{h,a}^{-1}(\ddot{r}_h - \dot{J}_{h,a}\dot{q}_a + \Psi_a) \\ & \quad + J_{\lambda,a}^T J_{\lambda,e}^{-T} M_e J_{\lambda,e}^{-1} (J_{\lambda,a}\dot{q}_a - \dot{J}_{\lambda,e}J_{\lambda,e}^{-1}J_{\lambda,a}\dot{q}_a) \\ & \quad - H_a + J_{\lambda,a}^T J_{\lambda,e}^{-T} H_e) + J_{u,a}^{-T} H_0 \end{aligned} \quad (21)$$

Here, $\Psi_a \in \mathbb{R}^8$ is a feedback control term, and $H_0 \in \mathbb{R}^8$ is the uncompensated internal force. Therefore, by defining the tracking error vector as

$$\varepsilon_a = [\varepsilon_{a,p}^T \quad \varepsilon_{a,d}^T]^T = [(y_a - r_{h,a})^T \quad (\dot{y}_a - \dot{r}_{h,a})^T]^T \quad (22)$$

Under the muscle control input, the control system of Eq. (16) can be defined as

$$M_{y,a}\dot{\varepsilon}_{a,d} = M_{y,a}\Psi_a + J_{h,a}^{-T}H_0 + J_{h,a}^{-T}W_a^T w - J_{h,a}^{-T}J_{\lambda,a}^T J_{\lambda,e}^{-T}J_{u,e}^T u_e \quad (23)$$

where $M_{y,a} = J_{h,a}^{-T} M J_{h,a}^{-1}$ remains as a positive definite matrix.

As the study focuses on the control of tremor at the wrist, by defining the wrist control error as

$$\varepsilon = [\varepsilon_p^T \quad \varepsilon_d^T]^T = [(\theta_a - \theta_{r,a})^T \quad (\dot{\theta}_a - \dot{\theta}_{r,a})^T]^T \quad (24)$$

and with the declaration of the selection matrices $J_s = [I_2, 0_{2 \times 6}]$ and $J_c = [0_{6 \times 2}, I_6]$, the inertia matrix can be decomposed as

$$M_{y,a} = \begin{bmatrix} M_s & M_c \\ M_c^T & M_r \end{bmatrix}; \quad M_s = J_s M J_s^T; \quad M_r = J_r M J_r^T \quad (25)$$

Therefore, the wrist error control system can be calculated as

$$M_e \dot{\varepsilon}_d = J_e(M_{y,a}\Psi_a + J_{h,a}^{-T}H_0 + J_{h,a}^{-T}W_a^T w - J_{h,a}^{-T}J_{\lambda,a}^T J_{\lambda,e}^{-T}J_{u,e}^T u_e) \quad (26)$$

where

$$J_e = [I_2 \quad -M_c M_r^{-1}]; \quad M_e = M_s - M_c M_r^{-1} M_c^T \quad (27)$$

Here, M_e is symmetric positive definite, which is proven based on the Schur complement: since $M_{y,a} = M_{y,a}^T > 0$, $M_e = M_s - M_c M_r^{-1} M_c^T = M_e^T > 0$. If M_e^{-1} is multiplied on both sides of the equation, we obtain $M_e^{-1} J_e = J_s M_{y,a}^{-1}$. The term J_e involves the coupled inertia at the floating base. However, based on Eqs. (8), (13), and (18) it can be shown that

$$J_{e,u}^T = -J_s J_{h,a}^{-T} J_{\lambda,a}^T J_{\lambda,e}^{-T} J_{u,e}^T = -J_e J_{h,a}^{-T} J_{\lambda,a}^T J_{\lambda,e}^{-T} J_{u,e}^T \quad (28)$$

This indicates that the inertia coupling effect does not affect u_e if it is guaranteed that the current constraint structure holds. Since $J_{e,u}$ is a purely kinematic term, the controller design via u_e can be realized if $J_{e,u}$ can be identified.

Finally, it is important to understand the possible cause of tremors based on the dynamic model. A final assumption is proposed to introduce stiffness and damping into the system: The term Ψ_a introduces stiffness into the system from the biomechanical structure and neural feedback loop [29–31], which leads to

$$\Psi_a = -K_a \varepsilon_{a,p} - B_a \varepsilon_{a,d} + \Psi_n(q_a, \dot{q}_a, \xi_a, \varepsilon_a) \quad (29)$$

where K_a and $B_a \in \mathbb{R}^{8 \times 8}$ are the stiffness and damping matrices, respectively; and $\Psi_n \in \mathbb{R}^8$ is the remaining nonlinear terms. Based on Eq. (29), Eq. (26) can be transformed into

$$M_e \dot{\varepsilon}_d = -M_e(K_s \varepsilon_p + B_s \varepsilon_d) + H_e + J_e J_{h,a}^{-T} W_a^T w + J_{e,u}^T u_e \quad (30)$$

with

$$\begin{aligned} K_s & = J_s K_a J_s^T; \quad B_s = J_s B_a J_s^T \\ H_e & = -M_e J_s (K_a J_r^T J_r \varepsilon_{a,p} + B_a J_r^T J_r \varepsilon_{a,d} + \Psi_n) + J_e J_{h,a}^{-T} H_0 \end{aligned}$$

Here, H_e is the gross internal force that comes from the stiffness coupled control input $-M_e J_s (K_a J_r^T J_r \varepsilon_{a,p} + J_s B_a J_r^T J_r \varepsilon_{a,d})$, the nonlinear stabilizing terms $M_e J_s \Psi_n$, and the uncompensated internal force H_0 . From Eq. (30), it can be noticed that H_e and $J_e J_{h,a}^{-T} W_a^T w$ together are uncertainties in the model. Overall, the proposed model in Eq. (30) is reasonable based on the assumptions that the tremor dynamics stem from internal perturbations, external

disturbances, and base excitations through the neurological and biomechanical systems featuring stiffness and damping effects. Based on this model, the following sections will discuss the control condition and controller design of the forearm-TAWE system.

4 Analysis and Identification of the Wrist Joint

The previous dynamic model demonstrated that the feasibility of TAWE is essentially determined by 2×2 input Jacobian matrix $J_{e,u}$ in Eq. (30), which is a purely kinematic term that represents mapping from the $[\theta_{e,1}, \theta_{e,2}]^T$ to $[\theta_{a,1}, \theta_{a,2}]^T$ under the kinematic constraints. This section discusses the effect of the wrist joint on the workspace of TAWE, and the acquisition of the estimation of $J_{e,u}$ through wrist kinematics regression for controller design.

In many studies, the wrist joint is modeled as sequenced rotational joints, where the FE and RUD motions are realized by one rotation followed by another. Some models simply approximated the wrist joint as a universal joint [32,33], where the FE and RUD rotations were orthogonal. Other models also took into consideration the offset between the FE and RUD axes and the translational displacements accompanying the FE and RUD motions [34–36]. There are also models that represent the wrist rotation with two pairs of universal joints [37]. In our analyses, the wrist joint is assumed as

$$T_{A1,A2} = T_{S1}T_{D1}(\theta_1^*)T_{S2}T_{D2}(\theta_2^*)T_{S3} \quad (31)$$

where

$$T_{S1} = \begin{bmatrix} R_{S1} & d_{S1} \\ 0 & 1 \end{bmatrix}; \quad T_{S2} = \begin{bmatrix} R_{S2} & d_{S2} \\ 0 & 1 \end{bmatrix}; \quad T_{S3} = \begin{bmatrix} I_3 & d_{S3} \\ 0 & 1 \end{bmatrix}$$

are constant transformations with R_S and d_S as constant rotation matrices and translational displacements. The default values (in millimeters) of d_S are obtained from the 3D design model as

$$d_{S1} = \begin{bmatrix} -6.3 \\ 70.0 \\ -41.0 \end{bmatrix}; \quad d_{S2} = \begin{bmatrix} 0 \\ 0 \\ 0 \end{bmatrix}; \quad d_{S3} = \begin{bmatrix} 1.0 \\ 62.0 \\ 28.0 \end{bmatrix} \quad (32)$$

The default values of all R_S matrices are set to $R_S = I_3$. The variable transformations are

$$T_{D1} = \begin{bmatrix} R_z((1-c_a)\theta_{a,1}^*)R_x(c_a\theta_{a,2}^*) & 0 \\ 0 & 1 \end{bmatrix} \\ T_{D2} = \begin{bmatrix} R_z(c_a\theta_{a,1}^*)R_x((1-c_a)\theta_{a,2}^*) & 0 \\ 0 & 1 \end{bmatrix} \quad (33)$$

where $\theta_a^* = [\theta_{a,1}^*, \theta_{a,2}^*]^T$ is the default generalized coordinates of the wrist (recall from Sec. 3.1 that there can be multiple candidates for θ_a), which may not be available to sensors; and $c_a \in [0, 1]$ is a constant parameter. Therefore, when $c_a = 0$, the wrist joint is a first-RUD-then-FE (RUD-FE) sequenced rotation model; $c_a = 1$ indicates the first-FE-then-RUD (FE-RUD) model; and the remaining indicates that the wrist rotation is constructed by two pairs of sequenced orthogonal rotations.

4.1 Wrist Joint and Exoskeleton Workspace. The validity of the workspace of TAWE is determined by the property of $J_{e,u}$. If $J_{e,u}$ has large eigenvalues, the actuators will have good input efficiency into the system. Any singularity that appears in $J_{e,u}$ will cause incapability in controlling full-wrist motion. Although it is shown in Fig. 2 that TAWE has adequate reachability in following wrist motion, valid control condition is not necessarily obtainable at every point in the workspace of TAWE. An important observation is that, for a fixed set of design parameters, the wrist model makes a huge difference in the workspace of TAWE. To

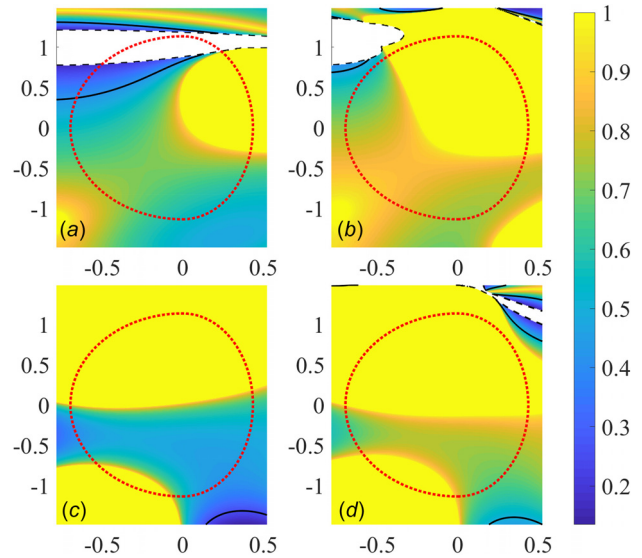


Fig. 5 Map of the eigenvalue norm ratio γ calculated from $J_{e,u}$ under different wrist models and design parameters, where (a) RUD-FE with $d_{y,5} = 0$, $d_{x,6} = 0$, (b) RUD-FE with $d_{y,5} = 3$ cm, $d_{x,6} = 1$ cm, (c) FE-RUD with $d_{y,5} = 0$, $d_{x,6} = 0$, and (d) FE-RUD with $d_{y,5} = 3$ cm, $d_{x,6} = 1$ cm; axes: horizontal—RUD (rad), vertical—FE (rad); black dash: $\kappa_1 < 0.25$; black solid: $\gamma < 0.25$; red dot: approximate wrist circumduction envelope

demonstrate this, we have compared the workspaces when TAWE is, respectively, coupled with the RUD-FE (at $c_a = 0$) and the FE-RUD (at $c_a = 1$) models. In both models, $\theta_a = \theta_a^*$, which indicates the transformation $T_{A1,A2}$ in the two models are different for identical θ_a values. The workspace condition is quantified by the ratio γ defined as

$$\gamma = |\kappa_1|/|\kappa_2| \quad (34)$$

where κ_1 and κ_2 are the two eigenvalues of $J_{e,u}$, which satisfies $|\kappa_1| \leq |\kappa_2|$. When $\gamma = 1$, the eigenvalues with the same norm; when $\gamma = 0$, $\kappa_1 = 0$, indicating that the workspace is invalid due to singularity.

Figure 5 compares the maps of γ calculated from the models under the RUD-FE and the FE-RUD wrist joints and different design parameters. An arbitrary contour of $\gamma = 0.5$ is drawn to separate the areas of inadequate control conditions. The vicinity area of singularity where $\kappa_1 < 0.25$ is considered a bad workspace. While the examined workspace is -85 deg to 85 deg in FE and -45 deg to 30 deg in RUD, the critical workspace is contained within the contour similar to the circumduction envelope, whose contour passes through -65 deg and 65 deg in pure FE motion as well as -40 deg and 25 deg in pure RUD motion.

In Fig. 5(a), there are no axle offsets ($d_{y,5}, d_{x,6} = 0$) between the Euler joint of the wrist exoskeleton. The singularity region cuts through the workspace when TAWE is coupled with the RUD-FE wrist joint. This problem was also witnessed previously in Ref. [23]. However, zero-offset works well for TAWE with the FE-RUD wrist model, as shown in Fig. 5(c). The Euler joint offset parameters ($d_{y,5}$ and $d_{x,6}$) are then modified. It is observed that by increasing $d_{x,6}$, the invalid workspace can be avoided in the case of the RUD-FE wrist joint. Doing so will, however, move the singularity region closer to the circumduction envelope in the FE-RUD cases. Increasing $d_{y,5}$ only slightly improves the control condition in the RUD-FE case. Finally, the parameter selection of $d_{y,5} = 30$ mm and $d_{x,6} = 10$ mm can provide satisfying workspace condition under both models as shown in Figs. 5(b) and 5(d).

This analysis demonstrates the effect of wrist kinematics on the control feasibility of the exoskeleton. It is also shown that tuning the design parameters may improve the control conditions. The

above observation may offer a direction to solving such problems in practice. A more general wrist model will also help in exploring design parameters that are more compatible with different user profiles.

4.2 Wrist Kinematics Identification. Section 4.1 discussed the structure of the wrist and its effects on the system's dynamics. As discussed earlier, the knowledge of the kinematic profile of the wrist is essential for control. The proposed controller accomplishes this through the regression of the wrist joint kinematics. The goal of the regression is to estimate $J_{e,a}$ by obtaining the missing information of the constraint Jacobian matrix $J_{\lambda,a,s}$ defined in Eq. (11).

The wearing locations of TAWE may change between each usage, which leads to different closed kinematic chains. Therefore, the regression needs to be carried out at the start of the system operation. This requires the regression to be efficient with only a limited amount of data. It is also desirable to consider only the directly measured position and orientation data for regression, as velocity data are more sensitive to noise and numerical errors if acquired indirectly. Under the assumption that the wrist joint model is time-invariant, it is possible to select the Euler angles as input variables of the regression. Therefore, the regression process can be separated into two independent parts:

- (1) The regression of d_w with the input variables Θ , with the regression structural function defined as

$$F_d(\Theta, p_d) = d_w \quad (35)$$

where p_d are the unknown parameters of the translational displacement regression model F_d .

- (2) The regression of the constraint relationship between Θ , with the regression structural function defined as

$$F_\Theta(\Theta, p_\Theta) = 0 \quad (36)$$

where p_Θ are the unknown parameters of the constraint regression model F_Θ .

While the two parts can be carried out in parallel, the final controller requires both regressions to be accurate. Recall that the default Euler angle sequence is the intrinsic z - y - x sequence. Therefore, it is possible to select $\theta_a = [\theta_z, \theta_x]^T$, so that $\theta_{a,1}$ and $\theta_{a,2}$ can quantify the RUD and FE motions, respectively. Thus, $J_{\lambda,a,s}$ can be calculated as

$$J_{\lambda,a,s} = J_{\lambda,\Theta} J_{\Theta,a} = \begin{bmatrix} J_{F,d}(\Theta, p_d) \\ J_{\xi,\Theta}(\Theta) \end{bmatrix} \begin{bmatrix} [0 \ 1] \\ J_{F,\Theta}(\theta, p_\Theta) \\ [1 \ 0] \end{bmatrix} \quad (37)$$

where the Jacobian matrices $J_{F,d}$, $J_{F,\Theta}$, and $J_{\xi,\Theta}$ are calculated from

$$\begin{aligned} \dot{d}_w &= J_{F,d} \dot{\Theta}; & \dot{\theta}_y &= J_{F,\Theta} \dot{\theta}_a \\ \dot{r}_{\lambda,\xi,2} &= J_{\xi,\Theta} \dot{\Theta} + [0_{3 \times 3} \ I_3] J_{\lambda,e,s} \dot{q}_e \end{aligned} \quad (38)$$

based on Eq. (10).

In general, the regression model has the structure of

$$F = F_1 + \sum_{i=2}^n c_i F_i \quad (39)$$

where F_1 is the main regression component; F_i are the supplemental regression components; and $c_i \in [0, 1]$ are the scaling constants that determine the weights of these components. Note that $c_i = 0$ implies exclusion of the component, which is necessary because in noisy cases, certain components may deteriorate the regression performance due to lack of robustness.

For the translational displacement regression, it is also desirable to have the regression affine parameters so that a single optimum can be guaranteed. The main regression component is designed as

$$F_{d,1} = p_{d,1} + R_\Theta(\Theta) p_{d,2} \quad (40)$$

which simply assumes that the wrist joint is a universal joint or a ball joint. The other components are

$$\begin{aligned} F_{d,2} &= P_{d,3} \sin(\Theta) + P_{d,4} \cos(\Theta) \\ F_{d,3} &= P_{d,5} \Theta + P_{d,6}(\Theta \star \Theta) \end{aligned}$$

where $P_{d,i} \in \mathbb{R}^{3 \times 3}$ are parameter matrices whose elements are unique and belong to p_d . As a result, the translational displacement regression model contains both specific and general features that may overcome some model uncertainties.

The first component of the rotational constraint regression model is selected by assuming that the rotation axis of ξ_w is always on a plane, which can be expressed as

$$F_{\Theta,1} = \text{Re}([0 \ 0 \ 1 \ 0]^T \times (\bar{\xi}_p(p_{\Theta,1}) \times \xi_{w,\Theta}(\Theta))) \quad (41)$$

Here, ξ_p is a preset rotation quaternion calculated from the parameter $p_{\Theta,1}$; and $\xi_{w,\Theta}$ is the quaternion ξ_w represented by Θ . Therefore, $F_{\Theta,1}$ will constrain the rotation axes of $\xi_{w,\Theta}$ on the x - z plane of a coordinate frame rotated by ξ_p .

An advantage of adopting $F_{\Theta,1}$ as the basis of F_Θ is that it is not affected by the rotation sequence of Θ , since Eq. (41) is formulated based on quaternions. Another advantage is that by adding a few terms to $F_{\Theta,1}$, it will be equivalent to certain sequenced rotation models. To demonstrate this, we define another Euler angle $\Phi = [\phi_x, \phi_y, \phi_z]^T$ calculated from

$$R_\Phi(\Phi) = R_{p,\Theta}(p_{\Theta,1})^T R_\Theta \quad (42)$$

where $R_{p,\Theta}$ is the rotation matrix converted from $p_{\Theta,1}$. By constructing a new constraint

$$r_\Phi(\Theta, \Phi) = F_{\Theta,1} + c_b \sin(\phi_x/2) \sin(\phi_z/2) \quad (43)$$

if Φ is calculated by the intrinsic z - y - x sequence, having $c_b = 1$ will constrain ϕ_y to 0; if Φ is calculated by the intrinsic x - y - z sequence, having $c_b = -1$ will constrain ϕ_y to 0. Therefore, by having

$$\begin{aligned} F_{\Theta,2} &= p_{\Theta,2}^T [\sin(\phi_x/2) \sin(\phi_z/2) \quad \cos(\phi_x/2) \cos(\phi_z/2)] \\ F_{\Theta,3} &= p_{\Theta,3}^T [\sin^2(\phi_x/4) \sin(\phi_z/2) \quad \sin^2(\phi_x/4) \cos(\phi_z/2)] \\ F_{\Theta,4} &= p_{\Theta,4}^T [\sin^2(\phi_z/4) \sin(\phi_x/2) \quad \sin^2(\phi_z/4) \cos(\phi_x/2)] \end{aligned} \quad (44)$$

there exist sets of parameters that make R_Θ based on F_Θ equivalent to the sequenced rotation models, such as the FE-RUD or RUD-FE models discussed in Sec. 4.1. In other cases, F_Θ based on the above formulation can approximate complicated rotation angles. It should be noted that due to the singularity in the rotation matrix converted from Euler angles, the Euler angle constraint regression is only applicable for small unknown preset angles.

The basis of the current dynamic nonlinear parameter estimator is the Levenberg-Marquardt (LM) algorithm [38], which is a combination of the gradient descent and Gauss-Newton methods that are effective for poor estimation cases and fast convergence near local minimum, respectively. Compared to many other algorithms, the LM algorithm is relatively simple and more time-efficient. The regression models will also provide the analytical expressions of the Jacobian with respect to the parameters, which is crucial to the regression process.

The traditional LM optimizer does not support bound constraints. To solve this problem, a constraint-violation penalty term can be added to the F_Θ . An example can be provided as

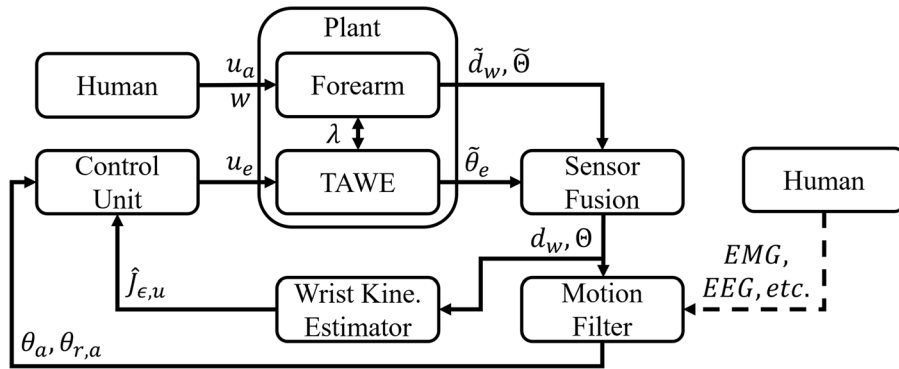


Fig. 6 The control system framework of TAWE

$$F_{\Theta,C} = \sum \sinh^{10}(p_{\Theta} * c_C) \quad (45)$$

where c_C is a constant vector that sets the bound for each p_{Θ} elements. This constraint component will set symmetric boundaries on the parameters without seriously affecting the cost function output when the parameters are small.

5 Controller Designs

The control framework that will be implemented on TAWE is illustrated in Fig. 6. The muscle input u_a and disturbance/perturbation w in the forearm are assumed to originate from the human user. To overcome inaccuracy from sensor noise and numerical errors, the 6DOF motion measurements $\tilde{\Theta}$, \tilde{d}_w , and $\tilde{\theta}_e$ collected by the IMUs and encoders will be fused using a Kalman filter [39] for a better state estimation. The states will then be fed into the kinematic model estimator to approximate $J_{\epsilon,u}$ to be used in the controller, which generates the control input u_e exerted by TAWE in the system.

The control framework also includes voluntary motion filtering, which is an important stage in practical application. As mentioned previously in Sec. 1, human motion filters can be a combination of methods (WFLC, BMFLC, autoregression, etc. [13,14,16]) designed for identifying the pattern of tremor and subtracting it from human motion θ_a . The identification may also require extra sensors (e.g., EMG, EEG) for exclusive information on human motion. As the current study mainly focuses on the kinematics and dynamics, the voluntary motion as the tracking reference $\theta_{r,a}$ is assumed to be available automatically in the upcoming simulation.

The controller design of the system is established on Eq. (30), in which many terms related to the dynamics of the systems are unknown. A preliminary controller can be designed based on the structure of

$$u_e = J_{\epsilon,u}^{-1}(-k_i \varepsilon_i - k_p \varepsilon_p - k_d \varepsilon_d - X_{u,1}(t, q, \dot{q})\hat{p}_{u,1} - X_{u,2}(t, q, \dot{q})\hat{p}_{u,2}) \quad (46)$$

where

$$\varepsilon_i = \int_0^t \varepsilon_p(\tau) d\tau \quad (47)$$

is the integral error; $k_i, k_p, k_d \geq 0$ are the proportional–integral–derivative (PID) control gains; $\hat{p}_{u,1} \in \mathbb{R}^{4\eta}$ and $\hat{p}_{u,2} \in \mathbb{R}^3$ are the tremor suppression and external force compensation parameters, respectively, as an estimation of the true value $p_{u,1}$ and $p_{u,2}$ for adaptive control (η is a positive integer); $X_{u,1}(t, q, \dot{q}) \in \mathbb{R}^{2 \times 4\eta}$ and $X_{u,2}(t, q, \dot{q}) \in \mathbb{R}^{2 \times 3}$ is the adaptive model component matrix corresponding to the parameters. Different components from u_e are implemented in various cases: the

integral control and external force adaptive components are proposed for light-power augmentation—the operation mode designed for assisting human motion; and the tremor suppression component is designed for countering tremorous motions. However, the P and D controller are universally required in all cases.

A stable PID tracking controller requires achieving the Hurwitz [40] state matrix

$$A = \begin{bmatrix} 0 & I_2 & 0 \\ 0 & 0 & I_2 \\ -k_i M_\varepsilon^{-1} & -k_p M_\varepsilon^{-1} & -k_d M_\varepsilon^{-1} \end{bmatrix} \quad (48)$$

Provided that the eigenvalues of M_ε^{-1} are $\kappa_{m,1} > 0$ and $\kappa_{m,2} > 0$, the six eigenvalues κ_c of A can be solved from

$$\begin{aligned} (\kappa_c^3 + k_d \kappa_{m,1} \kappa_c^2 + k_p \kappa_{m,1} \kappa_c + k_i \kappa_{m,1}) &= 0 \\ (\kappa_c^3 + k_d \kappa_{m,2} \kappa_c^2 + k_p \kappa_{m,2} \kappa_c + k_i \kappa_{m,2}) &= 0 \end{aligned} \quad (49)$$

According to Routh–Hurwitz criteria, the eigenvalues will have stable real parts when $k_d k_p \kappa_m > k_i$ for both $\kappa_{m,1}$ and $\kappa_{m,2}$. Therefore, the PID controller can only be applied with a good estimation of the range of κ_m , which is challenging when the user is performing multiple tasks.

Both external force compensation and tremor suppression control components adopt the model reference adaptive control (MRAC) structure. The main purpose of using this control component is to counter the torque created by gravitational forces. The external force is assumed to be acting on a point located away from the wrist. The generalized form of this force can be modeled as

$$X_{u,1} p_{u,1} = (J_{\omega,\Theta} J_{\Theta,d}^T \text{skew}([0 \ 0 \ 1]^T) R_{\Theta} p_{u,1}) \quad (50)$$

where $J_{\omega,\Theta}$ is the Jacobian matrix that satisfies $\omega = J_{\omega,\Theta} \dot{\Theta}$. If all the velocity-related internal forces (e.g., Coriolis forces, centripetal forces, and damping forces) are negligible during low-speed operations, the identified parameter norm $\|p_{u,1}\|$ will approximately be the moment of the gross system gravitational forces with respect to the approximate FE and RUD rotation.

Similar to the idea of BMFLC [14], by considering all the model terms as periodic system inputs identified within a known range of frequency, the equivalent gross input $X_{u,2} p_{u,2}$ can be constructed as

$$X_{u,2} p_{u,2} = \begin{bmatrix} \sum_{i=1}^{\eta} (\sin(\omega_i t) p_{u,2,i} + \cos(\omega_i t) p_{u,2,i+\eta}) \\ \sum_{i=1}^{\eta} (\sin(\omega_i t) p_{u,2,i+2\eta} + \cos(\omega_i t) p_{u,2,i+3\eta}) \end{bmatrix} \quad (51)$$

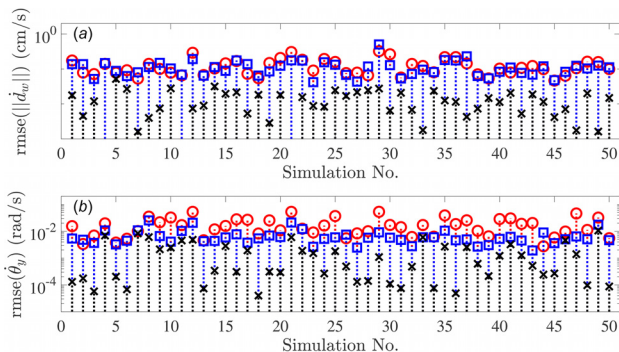


Fig. 7 Root-mean-square of estimation error of (a) d_w and (b) θ_y based on random design parameters and motion trajectories, where regressions are based on (1) black cross—zero-noise data; (2) red circle—noisy data; and (3) blue square—low-pass filtered data

which is the combination of sinusoidal waves at different frequencies, which is assumed to be the structures of the tremors. An advantage of this adaptive model is its capability of adapt to tremor signals with multiple dominant frequencies, provided that the range of ω_i contains these main frequencies.

If the proposed adaptive models are accurate, the error control system can be assumed as

$$\dot{\varepsilon} = - \begin{bmatrix} 0 & 1 \\ k_p M_e^{-1} & k_d M_e^{-1} \end{bmatrix} \varepsilon + \begin{bmatrix} 0 \\ M_e^{-1} (X_u p_u - X_u \hat{p}_u) \end{bmatrix} \quad (52)$$

where $X_u = [X_{u,1}, X_u, 2]$ and $p_u = [p_{u,1}^T, p_{u,2}]^T$. Therefore, the estimation parameter can then be updated as

$$\dot{\hat{p}}_u = -\Gamma_u^{-1} X_u^T (c_V \varepsilon_p + \varepsilon_d) \quad (53)$$

where $c_V \in \mathbb{R}_+$ is a constant parameter; and $\Gamma_u \in \mathbb{R}^{(4\eta+3) \times (4\eta+3)}$ is the symmetric positive definite adaptive update gain. Thus, a candidate adaptive control Lyapunov function can be chosen as

$$\begin{aligned} V = & \varepsilon_p^T (k_p + c_V k_d - c_V^2 M_e) \varepsilon_p \\ & + (p_u - \hat{p}_u)^T \Gamma_u (p_u - \hat{p}_u) \\ & + (c_V \varepsilon_p + \varepsilon_d)^T M_e (c_V \varepsilon_p + \varepsilon_d) \end{aligned} \quad (54)$$

Provided that controller design condition $k_d > c_V / \min(\kappa_m)$ that guarantees the positiveness of V based on the

$$\begin{aligned} k_d > c_V / \min(\kappa_m) & \rightarrow k_d z^T z > c_V z^T z / \min(\kappa_m) \\ & \geq c_V z^T M_e z \end{aligned} \quad (55)$$

where $z \in \mathbb{R}^2$ is a random vector.

Finally, it should be noted that all of the controllers at the current stage are only suitable for assisting slow human motions, in which cases it can be assumed that $\dot{M}_e \sim 0$. Under this condition, the stability of Eq. (54) can be proved by evaluating the time-derivative of V

$$\begin{aligned} \dot{V} = & 2\varepsilon_p^T (k_p + c_V k_d - c_V^2 M_e) \varepsilon_d - 2(p_u - \hat{p}_u)^T \Gamma_u \dot{\hat{p}}_u \\ & - 2(c_V \varepsilon_p + \varepsilon_d)^T (k_p \varepsilon_p + k_d \varepsilon_d + X_u (p_u - \hat{p}_u)^T \\ & - c_V M_e \varepsilon_d) \\ \leq & -2c_V k_p \varepsilon_p^T \varepsilon_p - 2(k_d - c_V / \min(\kappa_m)) \varepsilon_d^T \varepsilon_d \\ & - 2(p_u - \hat{p}_u)^T (\Gamma_u \dot{\hat{p}}_u + X_u^T (c_V \varepsilon_p + \varepsilon_d)) \\ \leq & 0 \end{aligned} \quad (56)$$

that satisfies $\dot{V} = 0$ only when $\varepsilon_p, \varepsilon_d = 0$ and $\hat{p}_u = p_u$, which proves the stability of the controller under the above assumptions.

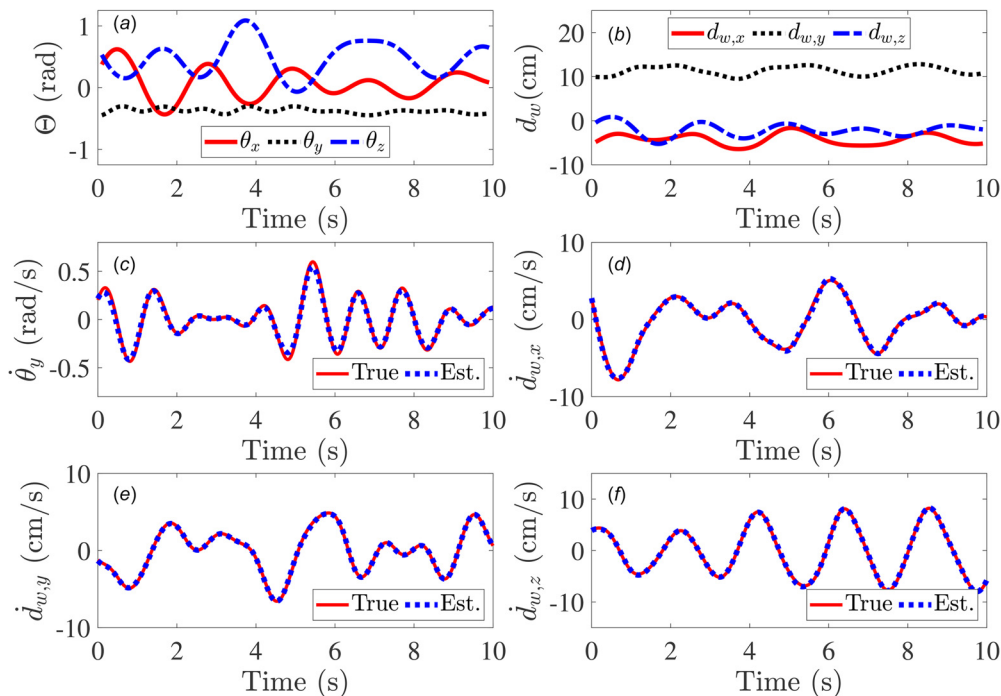


Fig. 8 Result of regression based on simulation configuration no. 29, where the regressor trajectories for training are shown in (a) Θ and (b) d_w ; and the comparison between true and estimated velocities of the testing trajectory are shown in (c) $\dot{\theta}_y$, (d) $d_{w,x}$, (e) $d_{w,y}$, and (f) $d_{w,z}$

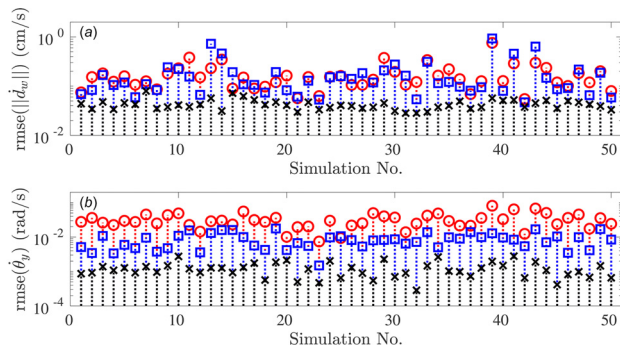


Fig. 9 Root-mean-square of estimation error of (a) d_w and (b) θ_y based on design parameters used in simulation no. 29 and motion trajectories, where regressions are based on (1) black cross—zero-noise data; (2) red circle—noisy data; and (3) blue square—low-pass filtered data

6 Simulation and Discussion

Simulations are carried out to validate the findings and study the performances of the methods. The results from the wrist kinematic identification are first presented, followed by the ones from the dynamics and control of TAWE.

6.1 Simulation on Regression Performance. The performances of the offline kinematic identification with the previously introduced regression models is studied quantitatively through simulation. To examine the overall performance, a total of 50 sets of random wrist model parameters (R_s , d_s , and c_a from Eq. (31)) and time trajectories of θ_a^* are generated for regression training. The wrist model parameters range within 1 cm in translational displacement and 10 deg in rotation angle, and the trajectories are contained within the anatomically possible range of wrist motion (± 20 deg in $\theta_{a,1}^*$ and ± 30 deg in $\theta_{a,2}^*$). Each set of θ_a^* trajectories is generated at a sampling rate of 200 Hz for 10 s, which is then used to generate the 6DOF displacement and velocity trajectories based on the randomly parameterized wrist model in Eq. (31). The scaling constants in Eq. (39) are selected as

$$c_d = [1 \ 0]; \quad c_\Theta = [10^{-1} \ 10^{-2} \ 10^{-2}] \quad (57)$$

For the current complexity of wrist model, it is only necessary to keep $F_{d,1}$. The unknown parameters p_d and p_Θ are initial set as zeros. Random noises are also added into the displacement data for regression process (-1 deg to 1 deg for Θ and $-0.25 \sim 0.25$ cm for d_w). Regression training are then carried out with respect to the zero-noise, noisy, and low-pass filtered version of each set of data.

For each of the 50 sets of random model parameters and trajectories, the regression performance is then evaluated by 20 other randomly generated 10-s θ_a^* trajectories. As the goal is to identify the Jacobian matrices, the evaluation is carried out with the zero-noise velocity trajectories— Θ is used to estimate d_w , and $[\dot{\theta}_x, \dot{\theta}_z]$ are used to estimate $\dot{\theta}_y$. The result overview is shown in Fig. 7, which demonstrates the root-mean-square errors of the velocity estimation. In general, the regression performs very well when there is no noise, as the upper bounds are approximately ± 10 cm/s in d_w and ± 1 rad/s for $\dot{\theta}_y$. The regression model also possesses robustness to overcome light noise with the LM optimizer. It is observed that noise significantly reduces the estimation accuracy, and filtering the noise visibly improves the Euler angle constraint regression. There is no apparent correlation between the d_w and Θ regressions, or between the zero-noise and the noisy regressions.

It appears that estimation errors in simulation no. 29 from Fig. 7 are relatively large. In this configuration, $c_a = 0.88$, indicating that the wrist joint is not an orthogonal joint. To understand whether the regression is poor due to the wrist model parameters or due to random trajectory/noise, the regression model is trained based on another 50 sets of random trajectories, with respect to the wrist model used in simulation no. 29. A single velocity estimation simulation of the regression model trained-based noisy data is presented in Fig. 8, where the real and estimated velocity trajectories of $\dot{\theta}_y$ and d_w are approximately identical. Figure 9 shows the performance overview of the regression model trained with respect to the simulation no. 29 wrist model. It is shown that there are many trails where the performance is acceptable. The relatively poor regression performances in the few cases are therefore likely related to random noises. The performance of regression models trained based on zero-noise data remains better than those trained based on noisy data.

The simulations demonstrated that the regression model can approximate a variety of complex wrist joint model. The regression model is also robust enough to deal with a certain level of noise. It should be noted that the regression models are all optimized offline based on 10-s trajectory data. The adopted method is, therefore, a strong preliminary approach for kinematic identification studies.

6.2 Simulation on Dynamics and Control. The first simulation on the dynamics and control of TAWE validates the proposed dynamical model by comparing the dynamical behaviors of the forearm–TAWE assembly modeled in two different engines—ANDY (an analytical multibody toolbox [41] in MATLAB) and V-REP [42], which uses a different approach in simulating multibody systems with kinematic constraints. The same default positions are set for both simulations as demonstrated in Fig. 10. As the primary goal is to verify the analytical model established in

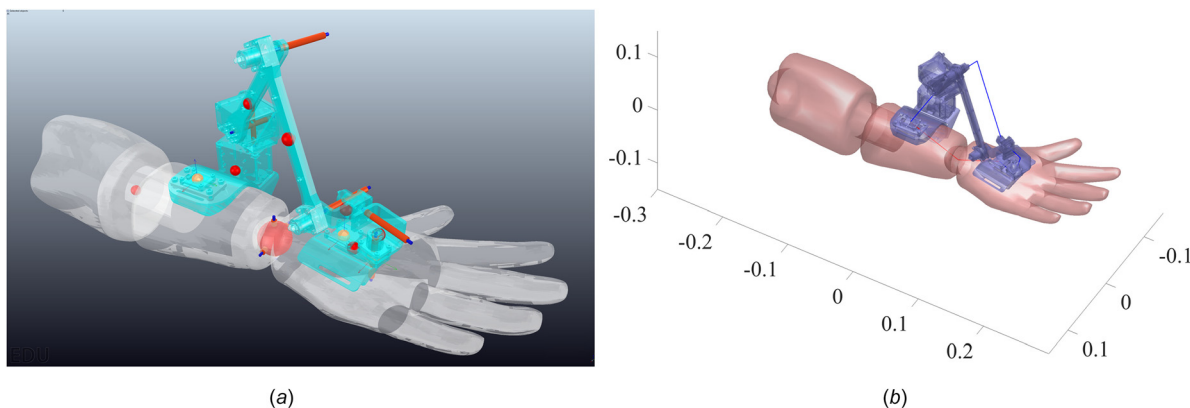


Fig. 10 Three-dimensional models from the simulations in (a) V-REP and (b) ANDY

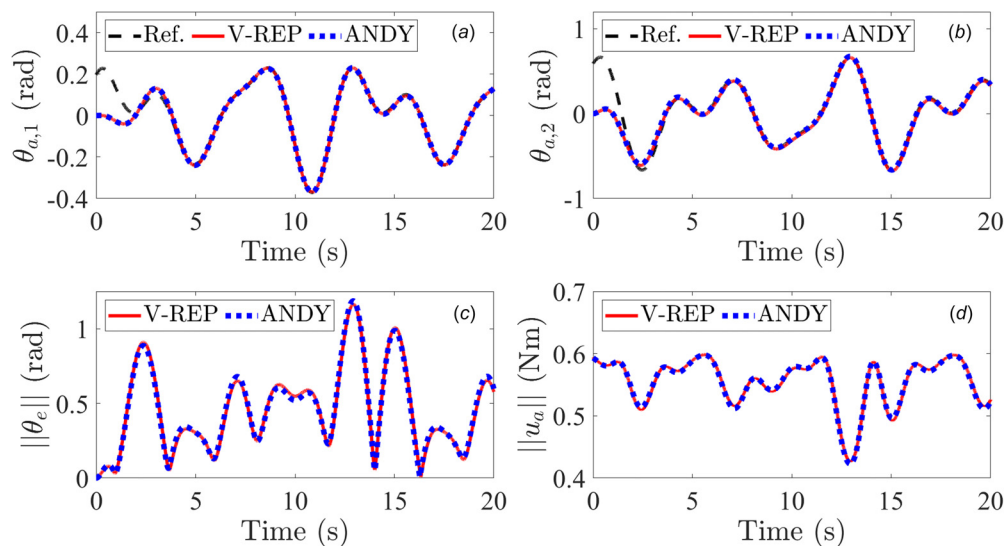


Fig. 11 Simulation validation between the dynamical models in V-REP and ANDY, where the subplots displays: (a) the tracking trajectory of $\theta_{a,1}$, (b) the tracking trajectory of $\theta_{a,2}$, (c) the norm of tracking error $\|\theta_e\|$, and (d) the norm of input $\|u_a\|$

Sec. 3 (the specific modeling process is realized with ANDY), a control input u_a in each simulation is generated to track the same planned reference. While the PD feedback components are designed based on states from each simulation, the feedforward controllers in both simulations are calculated based on the analytical model in ANDY. The result is shown in Fig. 11, from which it is apparent that the responses and control inputs from both systems are approximately identical. This indicates the viability of the analytical model, which is then used for the upcoming simulations.

The performances of controllers for light-power motion augmentations are simulated and compared. In this simulation, the forearm base is fixed in space, and there are no human inputs into the system ($w_a, u_a = 0$). Three different controllers are implemented—a PID controller with the real value of $J_{e,u}$, a PID controller with the estimation $\hat{J}_{e,u}$, and a PD + external force compensation MRAC controller with the estimated $\hat{J}_{e,u}$. The PID control gains are selected as $k_i = 0.25$, $k_p = 1$, and $k_d = 0.75$ ($k_i = 0$

for PD controllers). For the current model where the hand is approximately 0.65 kg, it is calculated that $\min(\kappa_m) > 100$ in workspace, which indicates that the control conditions in Eqs. (48) and (55) are easy to satisfy. The performances of trajectory tracking are shown in Fig. 12, where all the controllers have been demonstrated to be capable of following the reference. It should be noted in subplots (a) and (b) that the control performance are almost identical as $\hat{J}_{e,u}^{-1} J_{e,u} \sim I$. The trajectories of the position error norm $\|\varepsilon_p\|$ demonstrates that the MRAC controller is more effective than the PID controller in overcoming model uncertainties.

For the tremor control simulation, the system is again configured as floating-base and u_a is designed to hold the system at its default position. The source of the tremor as the periodic disturbance w_a consists of 17 different harmonic waves with frequencies ranging from 4 to 8 Hz acting on the system, resulting in vibrations. The performances of the passive (PD only) and active (PD + tremor suppression MRAC control) tremor suppression

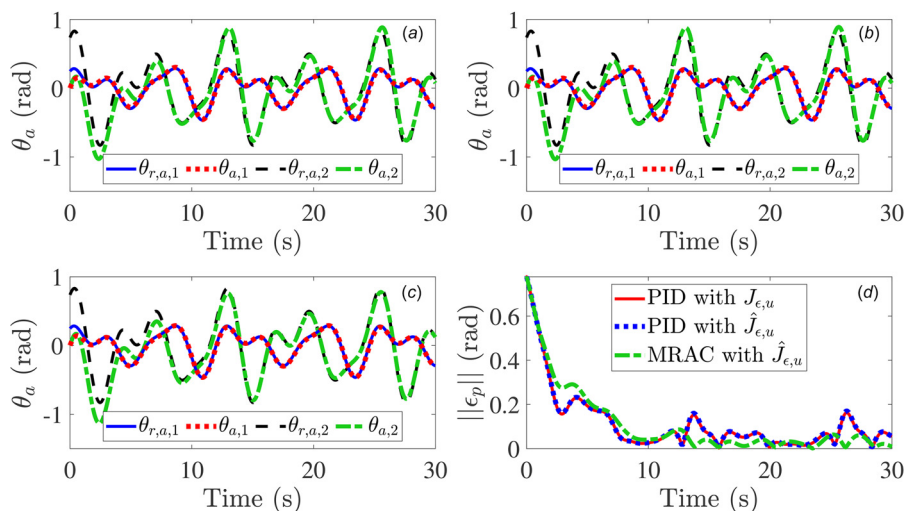


Fig. 12 The comparison of controllers for light-power motion augmentation. The first three subplots are the θ_1 trajectories based on the controllers—(a) PID with $J_{e,u}$, (b) PID with $\hat{J}_{e,u}$, and (c) PD + Adaptive with $\hat{J}_{e,u}$; and subplot (d) shows the norm of the tracking error $\|\varepsilon_p\|$.

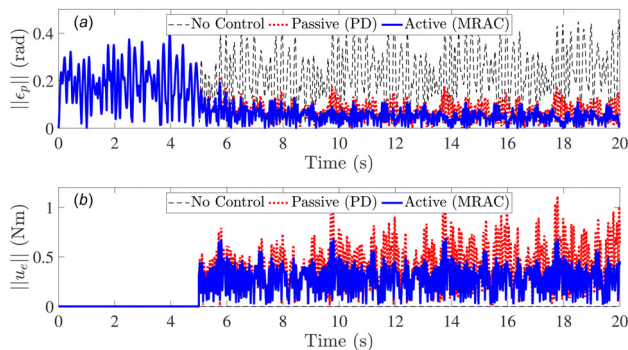


Fig. 13 The comparison of tremor suppression controllers, where subplot (a) compares tremor suppression control error $\|e_p\|$, and the subplot (b) compares the norm of input $\|u_e\|$

controllers are compared. In the active tremor suppression controller, the adaptive model consists of sinusoidal components at nine different frequencies ranging from 4 to 8 Hz. These tremor controllers are activated after $t=5$, allowing the uncontrolled tremorous vibration to enter the steady-state. The result is presented in Fig. 13, where it is clear from the plots of $\|e_p\|$ that active suppression has the best performance. The nine sinusoidal components in the adaptive model are not able to completely fit the dynamics of the disturbance, resulting in the tremor not being fully suppressed. Finally, the trajectories of $\|u_e\|$ indicate that active tremor suppression employs larger torque inputs, which consumes more power as expected.

7 Conclusion and Future Works

This study presented the theoretical analysis of TAWE—a novel exoskeleton designed for tremor alleviation in the wrist FE and RUD motions. To investigate the feasibility of TAWE, an analytical multibody model of the forearm–exoskeleton system was formulated, based on the coupling of two floating base subsystems. Based on the control system established from the multibody model, we observed that the information of the wrist kinematics is crucial to the application of TAWE. It was demonstrated that the structure of the wrist joint can significantly affect the control conditions of TAWE in its workspace. It was also shown that workspace conditions can be improved by tuning the design parameters. Later, a model was developed for the kinematic identification of the wrist, which was proved to be capable of robustly regressing complex wrist joint models based on noisy regressor data. After obtaining the wrist model, a control framework was established with controllers designed for tremor suppression and light-power motion augmentation. Through cross-platform numerical simulations, the analytical dynamical model is validated. Simulations have also shown that controllers can successfully provide movement assistance and active tremor suppression.

Overall, the study explored a few possible challenges in developing a full-wrist tremor suppression exoskeleton and provided solutions based on reasonable theoretical assumptions. However, more investigations are required before the full implementation of TAWE. A few potential future research direction are:

- (1) Establishing a more thorough study in the wrist kinematics and developing an online regression algorithm. This will be very useful considering that the real wrist kinematic model has a more complicated structure and may involve time-variant elements.
- (2) Exploring possible controllers to adapt to the inertia and other internal dynamical properties of the system. With a better knowledge of the system information, the control performance can be greatly improved.

- (3) Developing efficient motion-filtering algorithms that can extract tremorous motions from voluntary human motions. This also requires a thorough analysis to fundamentally understand the dynamics of tremor.

Finally, it should be pointed out that the analysis approach in this paper may be applicable to other similar wearable rehabilitation devices. TAWE is currently under development and the exoskeleton will be implemented as a useful tool to better understand and control pathological tremors.

The mathematical notations used in this paper are listed as following:

Nomenclature

- I_n = identity matrix of a specific dimension n (fits along with its neighboring blocks if no dimension specified)
- $Z > 0$ = square matrix Z is positive definite
- \bar{z} = conjugation of quaternion z (4×1)
- $z_{m \times n} = A$ = $m \times n$ matrix with all elements as $z \in \mathbb{R}$ (fits along with its neighboring blocks if no dimension specified)
- $z_1 \times z_2$ = multiplications of quaternions z_1 (4×1) and z_2 (4×1)
- $\|Z\|_n$ = the induced n -norm of a matrix Z ($n=2$ if not specified)
- Z^{-T} = the transposed inverse of Z (since $(Z^{-1})^T = (Z^T)^{-1}$)
- $Z_1 * Z_2$ = multiply two same size matrices Z_1 and Z_2 by elements

References

- [1] Louis, E. D., 2001, "Essential Tremor," *New Engl. J. Med.*, **345**(12), pp. 887–891.
- [2] Benito-León, J., and Louis, E. D., 2006, "Essential Tremor: Emerging Views of a Common Disorder," *Nat. Rev. Neurol.*, **2**(12), pp. 666–678.
- [3] Jankovic, J., 2008, "Parkinson's Disease: Clinical Features and Diagnosis," *J. Neurol., Neurosurg. Psychiatry*, **79**(4), pp. 368–376.
- [4] Kalia, L. V., and Lang, A. E., 2015, "Parkinson's Disease," *Lancet*, **386**(9996), pp. 896–912.
- [5] Gnadinger, M., and Hans-Ulrich Mellinghoff, A. K.-L., 2011, "Parkinson's Disease and the Bones," *Swiss Med. Wkly.*, **141**, p. w13154.
- [6] Pons, J. L., 2008, *Wearable Robots: Biomechatronic Exoskeletons*, Wiley, Chichester, England.
- [7] Fromme, N. P., Camenzind, M., Riener, R., and Rossi, R. M., 2019, "Need for Mechanically and Ergonomically Enhanced Tremor-Suppression Orthoses for the Upper Limb: A Systematic Review," *J. Neuroeng. Rehabil.*, **16**(1), p. 93.
- [8] Loureiro, R. C., Belda-Lois, J. M., Lima, E. R., Pons, J. L., Sanchez-Lacuesta, J. J., and Harwin, W. S., 2005, "Upper Limb Tremor Suppression in Adl Via an Orthosis Incorporating a Controllable Double Viscous Beam Actuator," IEEE Nineth International Conference on Rehabilitation Robotics 2005 (ICORR 2005), Chicago, IL, June 28–July 1, pp. 119–122.
- [9] Roccon, E., Belda-Lois, J., Ruiz, A., Manto, M., Moreno, J. C., and Pons, J., 2007, "Design and Validation of a Rehabilitation Robotic Exoskeleton for Tremor Assessment and Suppression," *IEEE Trans. Neural Syst. Rehabil. Eng.*, **15**(3), pp. 367–378.
- [10] Taheri, B., 2013, "Real-Time Pathological Tremor Identification and Suppression in Human Arm Via Active Orthotic Devices," *Ph.D. thesis*, Southern Methodist University, Dallas, TX.
- [11] Huen, D., Liu, J., and Lo, B., 2016, "An Integrated Wearable Robot for Tremor Suppression With Context Aware Sensing," IEEE IEEE 13th International Conference on Wearable and Implantable Body Sensor Networks (BSN), San Francisco, CA, June 14–17, pp. 312–317.
- [12] Anouti, A., and Koller, W. C., 1995, "Tremor Disorders. diagnosis and Management," *West. J. Med.*, **162**(6), p. 510.
- [13] Riviere, C. N., Rader, R. S., and Thakor, N. V., 1998, "Adaptive Cancelling of Physiological Tremor for Improved Precision in Microsurgery," *IEEE Trans. Biomed. Eng.*, **45**(7), pp. 839–846.
- [14] Veluvolu, K. C., and Ang, W. T., 2011, "Estimation of Physiological Tremor From Accelerometers for Real-Time Applications," *Sensors*, **11**(3), pp. 3020–3036.
- [15] Tatinati, S., Veluvolu, K. C., Hong, S.-M., Latt, W. T., and Ang, W. T., 2013, "Physiological Tremor Estimation With Autoregressive (ar) Model and Kalman Filter for Robotics Applications," *IEEE Sens. J.*, **13**(12), pp. 4977–4985.
- [16] Bo, A. P. L., Poignet, P., and Geny, C., 2011, "Pathological Tremor and Voluntary Motion Modeling and Online Estimation for Active Compensation," *IEEE Trans. Neural Syst. Rehabil. Eng.*, **19**(2), pp. 177–185.
- [17] Li, Z.-M., Kuxhaus, L., Fisk, J. A., and Christophel, T. H., 2005, "Coupling Between Wrist Flexion–Extension and Radial–Ulnar Deviation," *Clin. Biomech.*, **20**(2), pp. 177–183.
- [18] Moore, D. C., Crisco, J. J., Trafton, T. G., and Leventhal, E. L., 2007, "A Digital Database of Wrist Bone Anatomy and Carpal Kinematics," *J. Biomech.*, **40**(11), pp. 2537–2542.

- [19] Aydoğ, E., Ekşioğlu, E., Çakıcı, A., and Yılmaz, Ö., 2005, "Hand Deformity in Parkinson's Disease: Case Report," *Rheumatol. Int.*, **25**(7), pp. 548–549.
- [20] Gupta, A., O'Malley, M. K., Patoglu, V., and Burgar, C., 2008, "Design, Control and Performance of Ricewrist: A Force Feedback Wrist Exoskeleton for Rehabilitation and Training," *Int. J. Rob. Res.*, **27**(2), pp. 233–251.
- [21] Rose, C. G., Pezent, E., Kann, C. K., Deshpande, A. D., and O'Malley, M. K., 2018, "Assessing Wrist Movement With Robotic Devices," *IEEE Trans. Neural Syst. Rehabil. Eng.*, **26**(8), pp. 1585–1595.
- [22] Perry, J. C., Rosen, J., and Burns, S., 2007, "Upper-Limb Powered Exoskeleton Design," *IEEE/ASME Trans. Mechatronics*, **12**(4), pp. 408–417.
- [23] Wang, J., Barry, O., Kurdila, A. J., and Vijayan, S., 2019, "On the Dynamics and Control of a Full Wrist Exoskeleton for Tremor Alleviation," *ASME Paper No. DSCC2019-9118*.
- [24] Salvia, P., Woestyn, L., David, J. H., Feipel, V., Van, S., Jan, S., Klein, P., and Rooze, M., 2000, "Analysis of Helical Axes, Pivot and Envelope in Active Wrist Circumduction," *Clin. Biomech.*, **15**(2), pp. 103–111.
- [25] Jan, S. V. S., Salvia, P., Hilal, I., Sholukha, V., Rooze, M., and Clapworthy, G., 2002, "Registration of 6-DOFs Electrogoniometry and ct Medical Imaging for 3D Joint Modeling," *J. Biomech.*, **35**(11), pp. 1475–1484.
- [26] Li, W., and Wang, J., 2013, "Effective Adaptive Kalman Filter for MEMS-IMU/Magnetometers Integrated Attitude and Heading Reference Systems," *J. Navig.*, **66**(1), pp. 99–113.
- [27] Diebel, J., 2006, "Representing Attitude: Euler Angles, Unit Quaternions, and Rotation Vectors," *Matrix*, **58**(15–16), pp. 1–35.
- [28] Fresk, E., and Nikolakopoulos, G., 2013, "Full Quaternion Based Attitude Control for a Quadrotor," *IEEE European Control Conference (ECC)*, Zurich, Switzerland, July 17–19, pp. 3864–3869.
- [29] Formica, D., Charles, S. K., Zollo, L., Guglielmelli, E., Hogan, N., and Krebs, H. I., 2012, "The Passive Stiffness of the Wrist and Forearm," *Am. J. Physiol.-Heart Circ. Physiol.*, **108**(4), pp. 1158–1166.
- [30] Stiles, R. N., 1980, "Mechanical and Neural Feedback Factors in Postural Hand Tremor of Normal Subjects," *J. Neurophysiol.*, **44**(1), pp. 40–59.
- [31] Durbaba, R., Cassidy, A., Budini, F., and Macaluso, A., 2013, "The Effects of Isometric Resistance Training on Stretch Reflex Induced Tremor in the Knee Extensor Muscles," *J. Appl. Physiol.*, **114**(12), pp. 1647–1656.
- [32] Lemay, M. A., and Crago, P. E., 1996, "A Dynamic Model for Simulating Movements of the Elbow, Forearm, and Wrist," *J. Biomech.*, **29**(10), pp. 1319–1330.
- [33] Duprey, S., Naaim, A., Moissenet, F., Begon, M., and Cheze, L., 2017, "Kinematic Models of the Upper Limb Joints for Multibody Kinematics Optimisation: An Overview," *J. Biomech.*, **62**, pp. 87–94.
- [34] Esmaeili, M., Gamage, K., Tan, E., and Campolo, D., 2011, "Ergonomic Considerations for Anthropomorphic Wrist Exoskeletons: A Simulation Study on the Effects of Joint Misalignment," *IEEE/RSJ International Conference on Intelligent Robots and Systems*, San Francisco, Sept. 25–30, pp. 4905–4910.
- [35] Esmaeili, M., Jarrassé, N., Dailey, W., Bürdet, E., and Campolo, D., 2013, "Hyperstaticity for Ergonomic Design of a Wrist Exoskeleton," *IEEE 13th International Conference on Rehabilitation Robotics (ICORR)*, Seattle, WA, June 24–26, pp. 1–6.
- [36] Biryukova, E., Roby-Brami, A., Frolov, A., and Mokhtari, M., 2000, "Kinematics of Human Arm Reconstructed From Spatial Tracking System Recordings," *J. Biomech.*, **33**(8), pp. 985–995.
- [37] Seth, A., Hicks, J. L., Uchida, T. K., Habib, A., Dembia, C. L., Dunne, J. J., Ong, C. F., DeMers, M. S., Rajagopal, A., Millard, M., Hamner, S. R., Arnold, E. M., Yong, J. R., Lakshminanth, S. K., Sherman, M. A., Ku, J. P., and Delp, S. L., 2018, "Opensim: Simulating Musculoskeletal Dynamics and Neuromuscular Control to Study Human and Animal Movement," *PLoS Comput. Biol.*, **14**(7), p. e1006223.
- [38] Marquardt, D. W., 1963, "An Algorithm for Least-Squares Estimation of Non-linear Parameters," *J. Soc. Ind. Appl. Math.*, **11**(2), pp. 431–441.
- [39] Haykin, S. S., 2014, *Adaptive Filter Theory*, Pearson Education Ltd., Harlow, England.
- [40] Skogestad, S., and Postlethwaite, I., 2007, *Multivariable Feedback Control: Analysis and Design*, Vol. 2, Wiley, New York.
- [41] Wang, J., Kamidi, V. R., and Ben-Tzvi, P., 2018, "A Multibody Toolbox for Hybrid Dynamic System Modeling Based on Nonholonomic Symbolic Formalism," *ASME Paper No. DSCC2018-9000*.
- [42] E., Rohmer, S. P. N., and Singh, M. F., 2013, "V-Rep: A Versatile and Scalable Robot Simulation Framework," *Proceedings of the International Conference on Intelligent Robots and Systems (IROS)*, Tokyo, Japan, Nov. 3–7, pp. 1321–1326.